The nearby eclipsing stellar system δ Velorum. III. Self-consistent fundamental parameters and distance

A. Mérand, P. Kervella, T. Pribulla, M. G. Petr-Gotzens, M. Benisty, A. Natta, G. Duvert, D. Schertl, M. Vannier

A&A 532, A50 (2011)
DOI: 10.1051/0004-6361/201116896

Astronomy & Astrophysics

The nearby eclipsing stellar system δ Velorum

III. Self-consistent fundamental parameters and distance⋆

A. Mérand[1], P. Kervella[2], T. Pribulla[3,4], M. G. Petr-Gotzens[5], M. Benisty[6], A. Natta[7,8], G. Duvert[9], D. Schertl[10], and M. Vannier[11]

[1] European Southern Observatory, Alonso de Cordova 3107, Casilla 19001, Vitacura, Santiago 19, Chile
e-mail: amerand@eso.org
[2] LESIA, Observatoire de Paris, CNRS UMR 8109, UPMC, Université Paris Diderot, 5 place Jules Janssen, 92195 Meudon, France
[3] Astronomical Institute Slovak Academy of Sciences, 059 60 Tatranska Lomnica, Slovak Republic
[4] Astrophysikalisches Institut und Universitäts-Sternwarte, Schillergäßchen 2-3, 07745 Jena, Germany
[5] European Southern Observatory, Karl-Schwarzschild-Str. 2, 85748 Garching, Germany
[6] Max-Planck-Institut für Astronomie, Königstuhl 17, 69117 Heidelberg, Germany
[7] Osservatorio Astrofisico di Arcetri, INAF, Largo E. Fermi 5, 50125 Firenze, Italy
[8] School of Cosmic Physics, Dublin Institute for Advanced Studies, Dublin 2, Republic of Ireland
[9] UJF-Grenoble 1/CNRS-INSU, Institut de Planétologie et d'Astrophysique de Grenoble (IPAG) UMR 5274, Grenoble 38041, France
[10] Max-Planck-Institut für Radioastronomie, Auf dem Hügel 69, 53121 Bonn, Germany
[11] Laboratoire Fizeau, Université de Nice, CNRS-Observatoire de la Côte d'Azur, 06108 Nice Cedex 2, France

Received 15 March 2011 / Accepted 7 June 2011

ABSTRACT

Context. The triple stellar system δ Vel (composed of two A-type and one F-type main-sequence stars) is particularly interesting because it contains one of the nearest and brightest eclipsing binaries. It therefore presents a unique opportunity to determine independently the physical properties of the three components of the system, as well as its distance.
Aims. We aim at determining the fundamental parameters (masses, radii, luminosities, rotational velocities) of the three components of δ Vel, as well as the parallax of the system, independently from the existing Hipparcos measurement.
Methods. We determined dynamical masses from high-precision astrometry of the orbits of Aab-B and Aa-Ab using adaptive optics (VLT/NACO) and optical interferometry (VLTI/AMBER). The main component is an eclipsing binary composed of two early A-type stars in rapid rotation. We modeled the photometric and radial velocity measurements of the eclipsing pair Aa-Ab using a self-consistent method based on physical parameters (mass, radius, luminosity, rotational velocity).
Results. From our self-consistent modeling of the primary and secondary components of the δ Vel A eclipsing pair, we derive their fundamental parameters with a typical accuracy of 1%. We find that they have similar masses, $2.43 \pm 0.02\,M_\odot$ and $2.27 \pm 0.02\,M_\odot$. The physical parameters of the tertiary component (δ Vel B) are also estimated, although to a lower accuracy. We obtain a parallax $\pi = 39.8 \pm 0.4$ mas for the system, in satisfactory agreement ($-1.2\,\sigma$) with the Hipparcos value ($\pi_{\rm Hip} = 40.5 \pm 0.4$ mas).
Conclusions. The physical parameters we derive represent a consistent set of constraints for the evolutionary modeling of this system. The agreement of the parallax we measure with the Hipparcos value to a 1% accuracy is also an interesting confirmation of the true accuracy of these two independent measurements.

Key words. binaries: eclipsing – stars: early-type – stars: rotation – stars: individual: δ Velorum (HD 74956) – techniques: high angular resolution – techniques: interferometric

1. Introduction

Early-type main-sequence stars exhibit a number of peculiarities that are usually not encountered in cooler stars: fast rotation, debris disks, enhanced surface metallicities (Am), magnetic fields and rapid oscillations (Ap and roAp stars), etc. Although stellar structure and evolution models are now quite successful in reproducing the observed physical properties of most A-type stars, the observational constraints on these models remain relatively weak, occasionally leading to surprising discoveries. An example is provided by the recent interferometric observations of the A0V benchmark star Vega, which confirmed that Vega, as previously shown by Gulliver et al. (1994), is a pole-on fast rotator near its critical velocity (Aufdenberg et al. 2006). The same interferometric observations showed that Vega harbors a hot debris disk within 8 AU from the star (Absil et al. 2006).

δ Vel (HD 74956, HIP 41913, GJ 321.3, GJ 9278) is a bright multiple star including at least three identified components, and is among our closest stellar neighbors, with a revised Hipparcos parallax of $\pi_{\rm Hip} = 40.5 \pm 0.4$ mas (van Leeuwen 2007). This object has many observational peculiarities. Firstly, it was discovered only in 1997 that δ Vel hosts one of the brightest of all known eclipsing binaries (Otero et al. 2000), with a remarkably long orbital period ($P \approx 45$ days). This eclipsing binary is also one of the very few that are easily observable with the naked eye ($m_V \approx 2$). The eclipsing pair was first resolved

⋆ Based on observations made with ESO telescopes at Paranal Observatory, under ESO programs 076.D-0782(B), 081.D-0109(B), 081.D-0109(C), 282.D-5006(A) and Arcetri GTO program 084.C-0170(C).

using optical interferometry by Kellerer et al. (2007). Secondly, δ Vel is known to have a moderate thermal infrared excess (e.g., Aumann 1985; Su et al. 2006), and *Spitzer* observations revealed a spectacular bow shock caused by the motion of δ Vel in a dense interstellar cloud (Gáspár et al. 2008). The presence of interstellar material was also reported by Hempel & Schmitt (2003), who observed two red-shifted absorbing components in absorption in the Ca II K line of probably interstellar origin. In Paper I of the present series, Kervella et al. (2009) confirmed that the infrared excess is essentially emitted by the bow shock, and not warm circumstellar material located close to the stars. In the framework of a search for resolved emission from debris disks, Moerchen et al. (2010) obtained thermal infrared images of δ Vel using the Gemini South telescope and the T-ReCS instrument, and detected a marginally resolved emission at $\lambda = 10.4\,\mu$m.

In Paper II, Pribulla et al. (2011) used a combination of high-resolution spectroscopy and photometric observations (from the SMEI instrument, attached to the Coriolis satellite) to derive an accurate orbital solution for the eclipsing binary δ Vel A, and estimated the physical parameters of δ Vel Aa and Ab. They identified the two eclipsing components as fast rotating stars, with respective masses of $2.53 \pm 0.11\,M_\odot$ and $2.37 \pm 0.10\,M_\odot$ ($\approx$4% accuracy), and estimated the mass of δ Vel B to be $\approx 1.5\,M_\odot$.

In spite of this recent progress, uncertainties remain on the fundamental parameters of the different components of the system, in particular on their exact masses. Taking advantage of the availability of NACO astrometry of the δ Vel A-B pair, and new interferometric observations from the VLTI/AMBER instrument, we propose here to revisit the system along two directions. In Sect. 2, we describe our new VLTI/AMBER interferometric data, as well as our re-analysis of the spectroscopic and photometric data previously used in Paper II. Section 2.2 is dedicated to the description of our self-consistent model, and the derivation of an improved orbital solution, physical parameters, and an independent distance. In Sect. 3 we employ NACO astrometry of the visual δ Vel A-B binary to obtain an improved orbital solution. Compared to our work presented in Paper II, this new analysis result is a clearer view and gives better confidence in the derived fundamental parameters of the system (for all three components), thanks to the redundant nature of our data and our independent determination of the distance.

2. The orbit and parameters of δ Vel Aa and Ab

2.1. Observations and data analysis

2.1.1. Interferometry

AMBER (Petrov et al. 2007), the three-telescope beam combiner of the VLTI, has the proper angular resolution to resolve the Aa-Ab pair. This instrument simultaneously combines three ATs (Auxiliary Telescopes) or three UTs (Unit Telescopes) of the VLT and operates in the near infrared (H and K band). It has a choice of spectral resolutions of $R \sim 35$, $R \sim 1500$ or $R \sim 15\,000$. For this study, we had data in low resolution ($H + K$ bands at $R \sim 35$) and medium resolution (H or K band, at $R \sim 1500$). We used baselines on the order of 100 m to obtain spatial resolution in the milli-arcsecond regime. These interferometric data have been collected in a dedicated program (ESO program 076.D-0782), and during Guaranteed Time (GTO) from the Arcetri Observatory. We here present a reduction of these data.

We reduced the data using the AMBER reduction package `amdlib3` (Chelli et al. 2009; Tatulli et al. 2007) and performed the calibration using stellar calibrators chosen in the catalog by Mérand et al. (2005) and a custom software that estimates and interpolates the transfer function of the instrument. For each night, we derived the separation of Aa and Ab using a χ^2 map as a function of the separation vector (two parameters). The other parameters, such as flux ratio or individual diameters, were set using simple hypotheses but their choice did not affect our final estimated angular separations significantly. The resulting separation vectors are listed in Table 1 in coordinate east- and northward (which correspond to the u and v axes in the projected baselines map). The error bars on these vectors were estimated in the χ^2 map.

Table 1. AMBER separation vectors (primary to secondary).

Date MJD	Eastward mas	Northward mas
53 427.09	-4.1 ± 0.4	7.3 ± 0.5
53 784.08	-6.5 ± 0.5	13.8 ± 0.3
54819.25	-7.3 ± 0.2	16.1 ± 0.2
54 832.12	2.7 ± 0.7	-6.4 ± 0.4
55 147.38	1.6 ± 0.5	-4.0 ± 0.5

Notes. For simplicity, error bars were estimated along E and N directions even though the true error is an ellipse with orientation dicted by the χ^2 map. Apparently, the ellipses have a small flattening, which makes the approximation relevant.

2.1.2. Photometry

We used the photometric data from the SMEI satellite, presented in Paper II. The available quantity is the relative flux normalized to the value outside of the eclipses, because there was no absolute calibration of SMEI data available. We corrected for the presence of the B component, which is in the field of view of SMEI. From our model of B, the expected flux ratio between B and Aab is 7.5% in the SMEI bandpass. The transmission of the instrument has a triangular shape that peaks at 700 nm, with a quantum efficiency around 47%, and falls to $\approx$5% at 430 nm toward the blue, and 1025 nm toward the red (Spreckley & Stevens 2008). We removed this contribution which, if not taken into account, would result in an underestimation of the depth of the eclipses. We also incorporated to our photometric dataset the photometric measurement we derived of Aab in the K-band (Paper I). We use this value in our fit as the only constraint in terms of absolute photometry.

2.1.3. Spectroscopy

The observables we derived from the visible spectroscopic data are the broadening functions (BF) presented in Paper II (see this reference for more explanations). These functions contain a lot of information: not only do they contain the radial velocities that result from the orbital motion, but also the broadening caused by the stellar rotation and the flux ratio in the considered band.

From the observed BF, it is possible to derive the $v \sin i$ from the two components. After a few experimentations using the stellar surface model we will present below, we found that the following ad-hoc function parameterizes the BF well for a star seen from the equator:

$$\frac{\mathrm{BF}(v)}{\mathrm{BF}(v_0)} = \left(1 - \cos\left(\left[1 - \left(\frac{v - v_0}{v \sin i}\right)^2\right] \times \pi/2\right)\right)^{\alpha}, \quad (1)$$

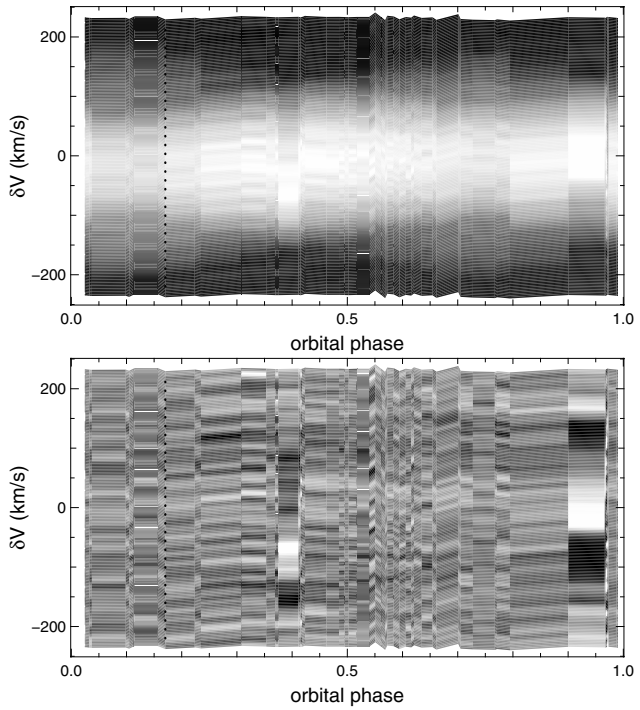

Fig. 1. δ Vel Aa-Ab spectroscopic broadening functions (BF). *Upper*: BF as a function of orbital phase; *Lower:* residuals after the fit. See Fig. 2 for the fit at the phase corresponding to the dotted line ($\phi \approx 0.17$). Our method to extract the radial velocity does not take into account the eclipses, as can be seen by the large residuals during the eclipses ($\phi \approx 0.40$ and $\phi \approx 0.97$, *upper right panel*).

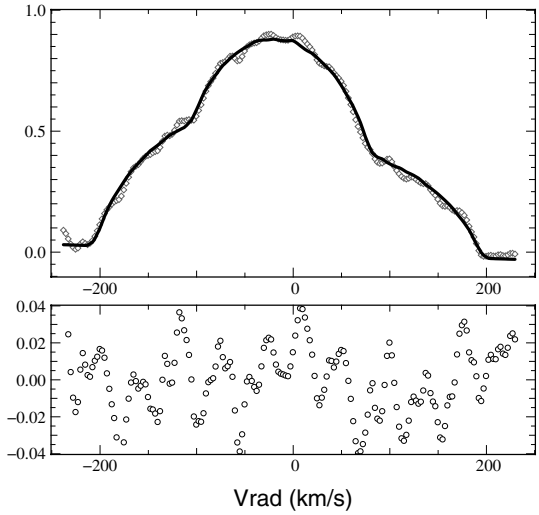

Fig. 2. Example of one fit of a broadening function (for the phase represented as a dotted line in Fig. 1, $\Phi \approx 0.17$). The analytical fit uses the sum of the two functions described in Eq. (1).

where α is the only parameter constraining the gravity darkening and v_0 is the velocity offset. The function is defined for $|v - v_0| \leq v \sin i$ only, and its value is 0 otherwise. Using this analytical model and a global fit, we estimated $v \sin i$ for each component and the radial velocities for each epoch (see Figs. 1 and 2 for the quality of the fit). We found $v \sin i$ to be 143.5 ± 0.2 km s^{-1} and 149.6 ± 0.2 km s^{-1} for Aa and Ab, respectively. Incidentally, we find $\alpha_a = 0.460 \pm 0.003$ and $\alpha_b = 0.451 \pm 0.003$. The rotation rate value is relatively independent of the actual gravity darkening (parameterized here by α) because it is set by the width of the broadening function, not its shape.

For our fit of the orbit and the stellar parameters, we did not use the center-to-limb darkening we derive here from the broadening functions. The surface brightness distribution is constrained by the photometric profile of the eclipses. However, a posteriori we will check the agreement between our best fit model and the limb-darkening derived in the analytical BF by modeling the BF from our model. See Sect. 2.2.3 and, more specifically, Fig. 7.

2.2. Global fit

2.2.1. Self-consistent model

In order to extract the fundamental parameters (masses, radii, surface temperatures, semi-major axis, etc.) from the observational data, we propose a self consistent modeling centered around the use of physical quantities: we model the system using two stars whose characteristics are computed based on their radii, total luminosities, and mass.

To illustrate the advantage of this approach, we can consider that to model the eclipses, we could use an ad-hoc model based on fractional radii (ratio to the semi-major axis) and brightness ratio, but this would not lead directly to the fundamental parameters of the system such as effective temperatures or luminosities. Our approach uses radii, masses, and luminosities: we obtain the fractional radii by self consistency between the semi-major axis based on Newton's form of Kepler's law (from the masses and the period of the orbit) and the measured apparent semi-major axis (constrained by interferometric separation vectors). The brightness ratio arises from the luminosity and radii and the photospheric models we use to model the surface of the stars.

Our stellar surface model also includes stellar rotation. We model the appearance of the star using a model developed contemporarily and similar to the one used in Aufdenberg et al. (2006) to model the interferometric visibilities of the star Vega. To compute the photometry, in particular during the eclipses, we generated synthetic images and integrated them to derive the light curves. The parameters we use are

- the total mass of the system (Aa+Ab);
- the fractional mass of Aa to the total mass of the eclipsing system (Aa+Ab);
- the physical radii of each component;
- the absolute luminosity of each component;
- the $v \sin i$ of each component, to parameterize the rotation.

In addition, we have the usual seven parameters for the visual orbit:

- the period;
- the date of passage at periastron;
- the eccentricity;
- three angles: inclination, ω and Ω;
- the apparent semi-major axis (in milliarcseconds).

The only parameterization of the physics of the two components is contained in the luminosity: the model we use of the stellar surface is the Roche approximation, which only uses the mass, radius, luminosity, and rotational velocity. Once the shape of the surface is computed, we link the local surface gravity and local effective temperature using the von Zeipel theory (see von Zeipel 1924, and Aufdenberg et al. 2006, for more details). The luminosity is constrained using several mechanisms: through the absolute photometry of the system, but also through the surface brightness that sets the depth of the eclipses.

The advantages of using the apparent semi-major axis compared to the physical quantity are simple. First of all, it is directly related to one of our observables: the interferometric separation vector. Secondly, we already have the semi-major axis by combining the Kepler's third law, the period, and the total mass. Combined with the angular semi-major axis, we derive a distance independently of the Hipparcos value (a brief discussion is presented in Sect. 2.3). The distance is derived internally in our model and used to extract a model apparent magnitude in the K-band, which is used as one of the constraints, we mentioned above.

We make the following assumptions:

- the stars have their rotation axis perpendicular to the plane of the orbit.
- We use a Von Zeipel gravity darkening coefficient of $\beta = 0.25$ in $T_{\rm eff} \propto g_{\rm eff}^{\beta}$, where $T_{\rm eff}$ and $g_{\rm eff}$ are the effective temperature and gravity at the surface. Even if recent observational constraints from Monnier et al. (2007) suggest $\beta \approx 0.19$, we chose to use von-Zeipel's classical value because it does not lead to qualitatively or quantitatively different results in our case.

2.2.2. Orbital and stellar derived parameters

The result of the global fit excellently agrees with all observed data that were used for the fit: the relative photometry of the eclipses (Figs. 3 and 4), the radial velocities (Fig. 5), and the separation vectors (Fig. 6). The corresponding orbital parameters and stellar parameters are presented in Tables 2 and 3.

2.2.3. *A posteriori* verifications

Our model is fairly simple and does not take into account one aspect: the heating of one star by the other's radiation. This effect could be important in our case under different conditions. The first one is if one star is heated by the other and develop a bright spot on its surface. We can discard this possibility because of there are no photometric variations outside the eclipses. The second case where the heating by the other star can be a problem is if this contribution is sufficient to modify the temperature structure of the stellar photosphere. We can check a posteriori that the radiation received from the other star is on the order of 3% of the radiation emitted (assuming similar surface brightness and a 2.5 $R_\odot$ star seen at a distance of 89 $R_\odot$). Approximating the surface as a blackbody, it corresponds to an increase of temperature of less than 1% ($1.03^{1/4}$). We thus assume to be correct our hypothesis: locally the photosphere can be approximated by an ATLAS model.

We can also check the consistency of our model beyond the fit of the data we presented. In particular, we can compare the predicted broadening functions based on our model and the broadening functions we observe because we did not implement the direct fit of the broadening function to our model. If we do so (Fig. 7), the comparison is very satisfactory, even though the wings of the data (represented by the analytical function fit to the data in the thick gray line) seem deeper than for the model. In other words, the gravity darkening of the model is slightly underestimated, but only by a small fraction, considering that a model without gravity darkening (small gray dots on Fig. 7) produces a very strong disagreement.

Investigating the possible causes of this problem, we realized that we can reproduce the more pronounced darkening of the equator compared to the pole by tilting the star to 10 degrees from the plane of the sky: this shifts the pole more to the line of sight of the observer and hence increases the contrast between the pole and the equator.

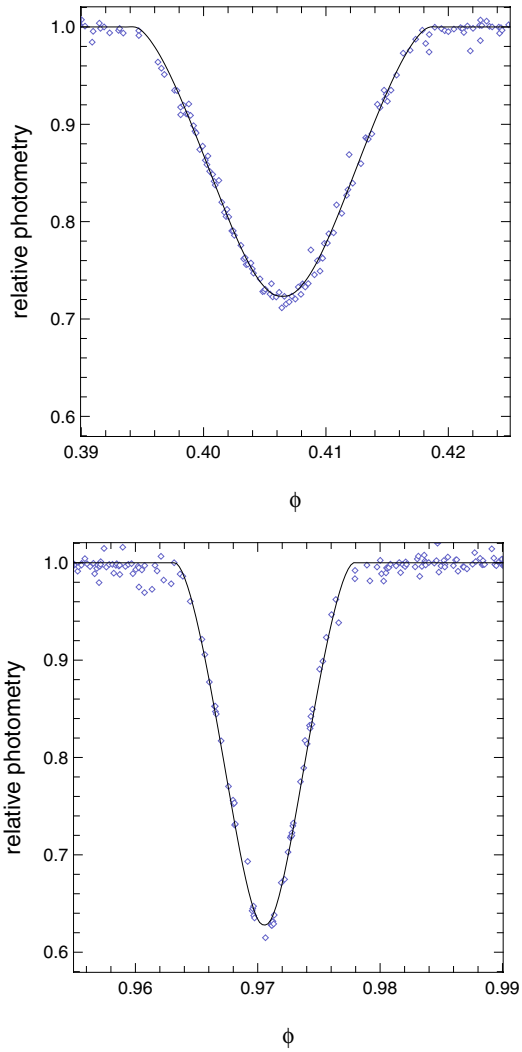

Fig. 3. δ Vel Aa-Ab SMEI photometric measurements (points) and fit of the eclipses (line) as a function of orbital phase: *the upper panel* is the the primary eclipse, *the lower panel* the secondary.

Forcing the inclination of the spin of the stars to be 80 degrees instead of 90 degrees does not dramatically change the fundamental parameters of the star estimated from our fit. One of the reasons is that it changes the sin(i) by only 1.5%, the actual rotational velocity is mostly unaffected. The fit also converges for aligned spins, with the fundamental parameters within the error bars of the one estimated in the case we presented in the main part of this work.

Our model's broadening function agrees well with the observations and thus confirms the consistency with the data. We also see that our model may slightly underestimate the gravity darkening, or, alternatively, the stars have their rotational axis tilted on the order of 10 degrees toward the observer, which does not qualitatively or quantitatively impact the fit of the data that led to the estimation of the fundamental parameters presented above.

Another test is to compare the predicted wide-band photometry with the observed ones. In the literature, there are a handful of data for the combined AB or A and B separately. If we compare these, we see (Table 4) that the bluest magnitudes are not reproduced well. Assuming a $B-V$ excess of $E(B-V) = 0.055$,

Table 2. Aa-Ab orbital and stellar parameters fitted to the photometric, interferometric and radial velocity data with our model.

	Aa	Ab	Constrained from
a (mas)	16.51 ± 0.16		interferometry
Total mass ($M_\odot$)	4.69 ± 0.03		all observations
$M_{\rm Aa}/(M_{\rm Aa} + M_{\rm Ab})$	0.516 ± 0.001		spectroscopy
Polar Radius ($R_\odot$)	2.79 ± 0.04	2.37 ± 0.02	photometry
Luminosity ($L_\odot$)	67 ± 1	51 ± 1	photometry
$v \sin i$ (km s^{-1})	143.5 ± 0.2	149.6 ± 0.2	spectroscopy
Period P (d)	45.1503 ± 0.0002		all observations
MJD$_0$ modulo P	19.159 ± 0.010		all observations
e	0.287 ± 0.001		all observations
i (deg)	89.04 ± 0.03		all observations
ω (deg)	109.79 ± 0.09		all observations
Ω (deg)	65.0 ± 0.6		interferometry
V_γ (km s^{-1})	-9.78 ± 0.07		spectroscopy
χ^2 $V_{\rm rad}$ Primary (err 0.75 km s^{-1})	1.13		
χ^2 $V_{\rm rad}$ Secondary (err 1.3 km s^{-1})	1.03		
χ^2 Photometry (err 0.75%)	1.15		
χ^2 Interferometry	1.05		

Notes. The last four lines present the agreement as reduced χ^2.

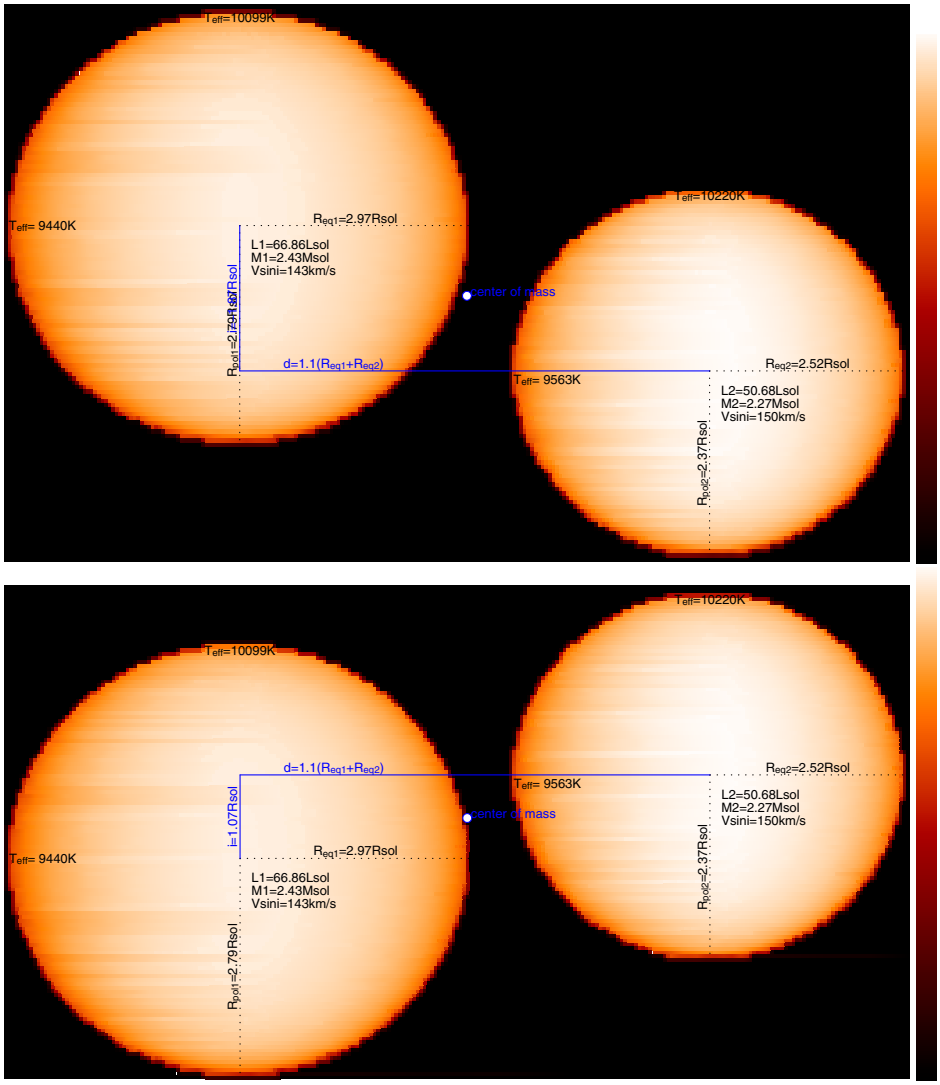

Fig. 4. δ Vel Aa-Ab synthetic images in linear scale, close to the eclipses: *the upper panel* is the configuration of the primary eclipse, *the lower panel* is the secondary eclipse.

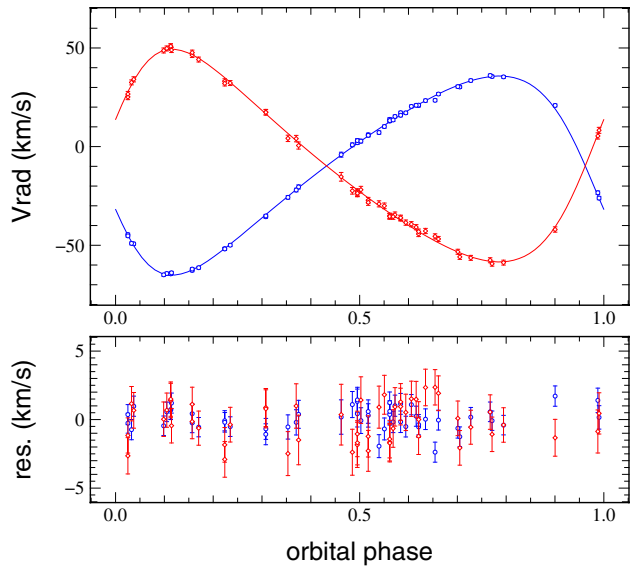

Fig. 5. δ Vel Aa-Ab radial velocities as a function of orbital phase, with the model from the fit overplotted and residuals plotted in *the lower panel*. Round points (blue) are for the primary and diamonds (red) for the secondary.

Table 3. Derived fundamental parameters for δ Vel Aa and Ab.

	Unit	δ Vel Aa	δ Vel Ab	Vega
Mass	$M_\odot$	2.43 ± 0.02	2.27 ± 0.02	2.3 ± 0.2
Luminosity	$L_\odot$	67 ± 3	51 ± 2	37 ± 3
Polar Radius	$R_\odot$	2.79 ± 0.04	2.37 ± 0.02	2.26 ± 0.07
Equ. Radius	$R_\odot$	2.97 ± 0.02	2.52 ± 0.03	2.78 ± 0.02
Polar $T_{\rm eff.}$	K	10 100	10 120	10 150
Equ. $T_{\rm eff.}$	K	9700	9560	7900
Avg. $T_{\rm eff.}$	K	9450	9830	9100
$\omega/\omega_{\rm crit.}$		0.61	0.60	0.91
Polar log(g)	cm s^{-2}	3.90	4.10	4.10 ± 0.1
Eq. log(g)	cm s^{-2}	3.78	3.99	3.65 ± 0.1
i	deg	~90	~90	4.7 ± 0.3
rotation rate	1/d	0.95	1.17	1.90
metallicity	[M/H]	−0.33[1]	−0.33[1]	−0.5[2]

Notes. Parameters for Vega are displayed for comparison and are adapted from Aufdenberg et al. (2006).

References. [1] Gray et al. (2006); [2] Castelli & Kurucz (1994).

the difference is nicely explained using an ISM extinction law as presented in Kervella et al. (2004).

2.3. Distance

Our parameterization allows us to derive the distance as the ratio between the semi-major axis of the eclipsing component (from the total mass, the period and Kepler's third law) and its apparent semi-major axis (from the interferometric observations). This distance estimate is particularly interesting because it is purely geometrical and independent of the Hipparcos measurement. From our model, we obtain a parallax of $\pi = 39.8 \pm 0.4$ mas for δ Vel.

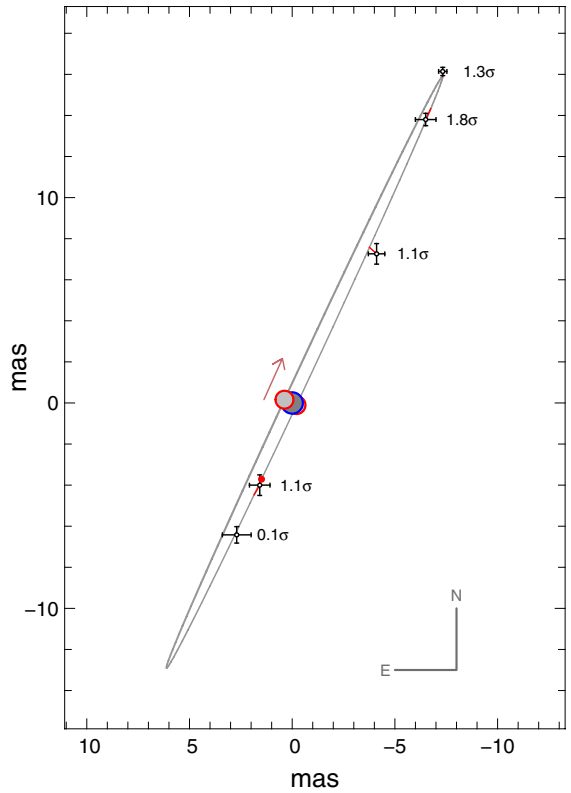

Fig. 6. δ Vel Aa-Ab visual orbit: AMBER positions (black dots with error bars, see Table 1); fitted orbit (gray line), Aa stellar disk (dark gray disk with blue surrounding), the position of Ab at periastron (red dot) and Ab stellar disks for the positions of the eclipses (gray disk with red surroundings). Residuals to the orbit (red lines, too small to see in most cases) and quality of the fit (in number of sigmas). The overall agreement corresponds to a reduced χ^2 of 1.05.

This value agrees well with the $\pi_{\rm Hip} = 40.5 \pm 0.4$ mas revised Hipparcos parallax[1] obtained by van Leeuwen (2007) within 1.2σ. This confirmation of the true accuracy of these independent measurements, at the 1% level, shows that the Hipparcos measurement was not disturbed by the binary nature of δ Vel A. This somewhat surprising result is due to the similar brightness ratio $L_{\rm Aa}/L_{\rm Ab} \approx 1.3$ and mass ratio $M_{\rm Aa}/M_{\rm Ab} \approx 1.1$ of the δ Vel A pair. This results in a very small apparent displacement of the center of light of the Aab system during the orbit, with respect to the center of gravity of the two stars. Using our model of the eclipsing system, we computed the expected photocenter displacement during a full orbit. We found that the peak-to-peak photocenter displacement is on the order of one milliarcsecond, which is much smaller than the apparent astrometric shift owing to the parallax. The binarity of the system therefore did not significantly bias the Hipparcos parallax measurement, neither did the low brightness of the B component. The observations of the photocenter displacement through high-precision differential astrometry with the VLT/NACO instrument will be the subject of a future article.

[1] The revised Hipparcos parallax is consistent within 1σ with the original Hipparcos reduction (40.9 ± 0.4 mas; ESA 1997), and with the ground-based parallax of this star (49.8 ± 9.4 mas; Van Altena et al. 1995).

Table 4. Computed and observed broad band photometry.

			Model (observation)			Δ	Extinction
band	Aa	Ab	Aab	B	AB	obs.-mod.	$E(B-V) = 0.055$
B	2.39	2.71	1.78	6.10	1.76 (*2.00*[1])	0.24	0.23
V	2.41	2.73	1.81	5.59 (*5.54*[2])	1.78 (*1.96*[1])	0.18	0.18
J	2.43	2.76	1.83	4.72	1.76 (*1.77*[3])	0.02	0.04
H	2.45	2.78	1.85	4.44	1.75 (*1.76*[3])	0.01	0.03
K	2.46	2.78	**1.85** (*1.86*[2])	4.42 (*4.40*[2])	1.76 (*1.72*[3])	–0.04	0.02

Notes. The magnitudes predicted by the best-fit model are listed together with the observed magnitudes (brackets). In bold is the K-magnitude of Aab, which was used to constrain our fit. The B column comes from the fit presented in Sect. 3. The last two columns are the observed differences and the expected extinction for $E(B-V) = 0.055$, which best fits the observed colors. Observed magnitudes are from Morel & Magnenat (1978)[1]; Paper I[2] and Skrutskie et al. (2006)[3].

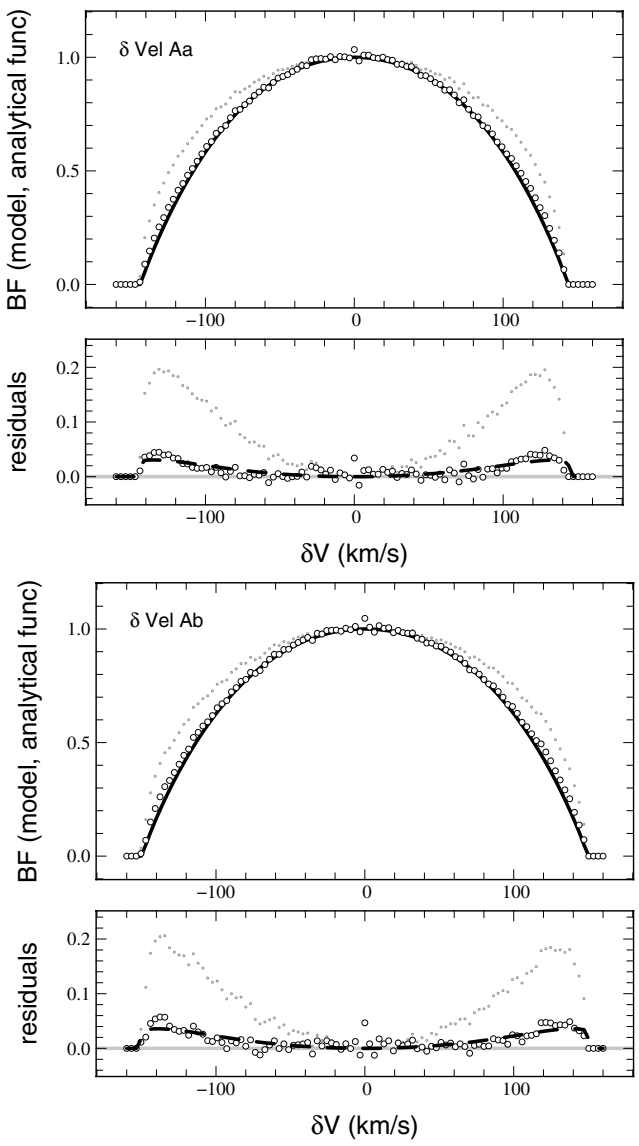

Fig. 7. δ Vel Aa-Ab expected broadening functions computed for our models. For each star (Aa and Ab), the open dots are for the model (Table 3) and the thick line is for the analytical function resulting from the fit to the spectroscopic data (Fig. 2). The small gray dots are for the model as well, but ignoring the gravity darkening. In the *small panels* we plot the residuals "model" – "fit on spectroscopic data", where the dashed line is the best fit of the model using the same analytical function, showing the slight underestimation of the gravity darkening by our model.

3. The orbit and parameters of δ Vel B

3.1. Astrometric data

The binarity of δ Vel was discovered by S. I. Bailey in 1894 from Arequipa, Peru (and independently by Innes 1895). Over more than one century, the separation between δ Vel A and B has been decreasing at a rate that nicely matches the progression of the angular resolution of the successive generations of imaging instruments (visual observations, photography, electronic devices). This progression allowed a relatively regular tracing of the visual orbit of the pair, down to the sub-arcsecond separations that occur around the periastron passage. With the advent of speckle interferometry (Tango et al. 1979) and the Hipparcos satellite (ESA 1997) the accuracy of the measured relative positions improved significantly. In Paper I we presented in detail the new data we obtained with the *Very Large Telescope*, using both the K-band adaptive optic system VLT/NACO (Rousset et al. 2003; Lenzen et al. 1998) and the N-band camera VLT/VISIR (Lagage et al. 2004). Thanks to the large aperture of the telescopes and the diffraction-limited angular resolution, these observations provide us with new high-precision astrometry of the A-B pair. The resulting separations of δ Vel B relatively to A are presented in Table 5. For the conversion of the separation measured in pixels to angular separations, we adopted the pixel scale of 13.26 ± 0.03 mas/pixel (Masciadri et al. 2003) for NACO and 75 ± 1 mas/pixel for VISIR. The assumed NACO plate scale agrees well with the calibration by Neuhäuser et al. (2008), who demonstrated that this figure is stable over a period of at least three years. The VISIR plate scale uncertainty is set arbitrarily to ≈1%, although it is probably better in reality. The angular separation was only ≈0.6″ for the epoch of our observations.

In addition to these new astrometric measurements, we also take advantage of the historical astrometric positions assembled by Argyle et al. (2002) in his Table 5, which includes 17 epochs between 1895 and 1999. These authors used the two speckle interferometry epochs from Tango et al. (1979) with a different definition for the projection angle, leading to an apparent inconsistency with the other measurements. Transforming the Tango et al. projection angle PA using PA → (180 − PA), these two data points become much more consistent with the other epochs and observing techniques.

3.2. Orbital elements

We adjusted the orbital parameters of the δ Vel A-B pair to the whole sample of astrometric data, and the result is presented graphically in Fig. 8. The corresponding orbital elements are listed in Table 6. Thanks to a semi-major axis twice more precise

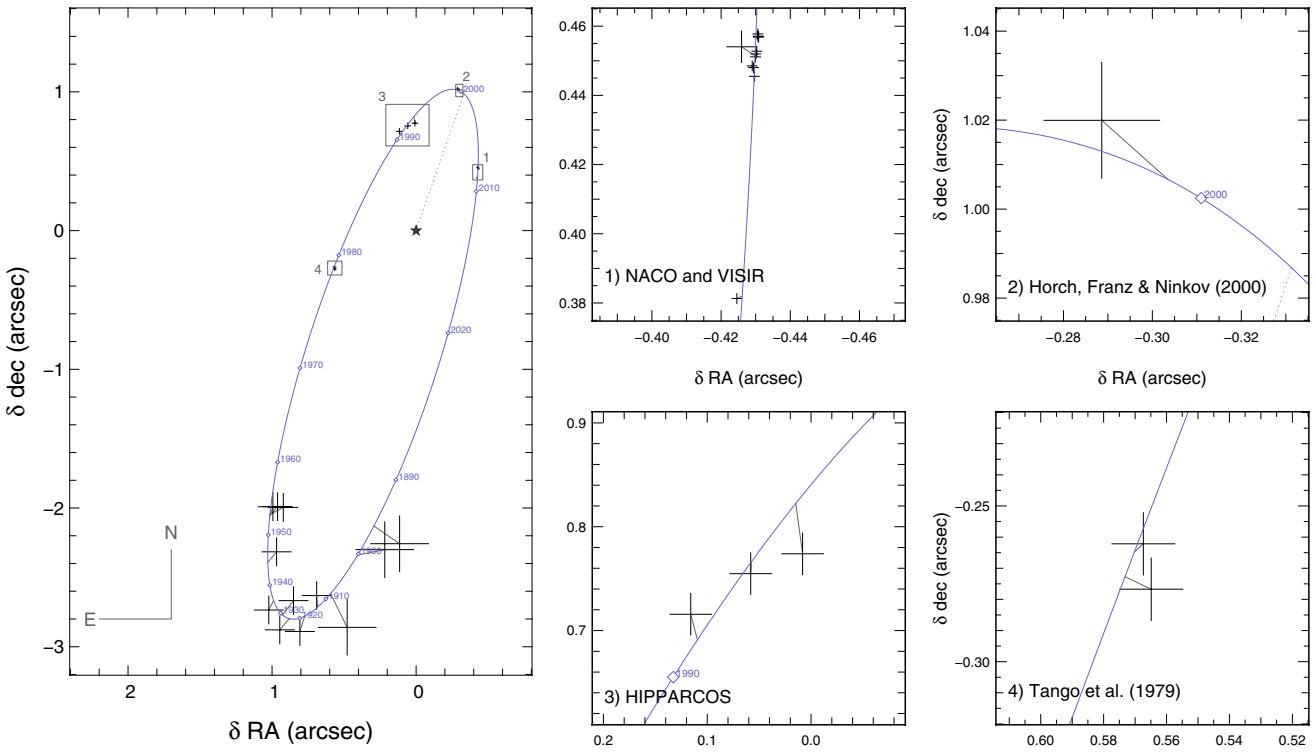

Fig. 8. *Left panel*: astrometric measurements of the relative position of δ Vel B (crosses) with respect to δ Vel A ($\star$ symbol), with our best-fit orbital solution (solid ellipse, see Table 6 for the orbital parameters). Thin lines connect each measurement to the corresponding point on the adjusted orbit. The dotted line corresponds to the periastron passage, and the diamonds correspond to the position of δ Vel B on January 1 every ten years between 1890 and 2020. *Right panels (labeled 1 to 4):* correspond to zooming boxes on the larger view. NACO and VISIR data (panel 1) are tabulated in Table 5; the data in panel 2 come from Horch et al. (2000); the data in panel 4 are from Tango et al. (1979). Zooming boxes' positions are reported on the main (*left*) panel.

Table 5. Differential astrometry of δ Vel from NACO and VISIR images.

UT date	MJD-54 000	$[\alpha_B - \alpha_A]$ mas	$[\delta_B - \delta_A]$ mas
2008-04-01^N	557.0224	-430.6 ± 1.0	457.8 ± 1.0
2008-04-04^N	560.9976	-430.7 ± 1.0	457.1 ± 1.0
2008-04-06^N	562.0121	-430.8 ± 1.0	457.1 ± 1.0
2008-04-07^N	563.0048	-430.7 ± 1.0	457.0 ± 1.0
2008-04-20^N	576.9715	-430.3 ± 1.0	452.9 ± 1.0
2008-04-23^N	579.0231	-430.0 ± 1.0	452.0 ± 1.0
2008-04-24^V	580.0503	-425.9 ± 4.3	454.0 ± 4.5
2008-04-24^N	580.9917	-429.8 ± 1.0	451.1 ± 1.0
2008-05-05^N	591.9748	-428.9 ± 1.0	448.7 ± 1.0
2008-05-07^N	593.9732	-429.2 ± 1.0	448.0 ± 1.0
2008-05-18^N	604.0442	-429.6 ± 1.0	445.4 ± 1.0
2009-01-07^N	838.1347	-424.6 ± 1.0	381.3 ± 0.9

Notes. Measurements from NACO have the symbol ^{N}, whereas measurements from VISIR have ^{V}. The angles are all expressed in milliarcseconds.

and a period ten times as precise, the total mass value derived from Kepler's third law is significantly improved, which becomes limited by our parallax estimate of $\pi = 39.8 \pm 0.4$.

$$M(\mathrm{Aab + B}) = 6.15 \pm 0.15_{\mathrm{orbit}} \pm 0.17_{\mathrm{parallax}}\, M_\odot. \quad (2)$$

3.3. Physical properties of δ Vel B

We used a spectral energy distribution (hereafter SED) fit to the photometric data (Table 7) corrected for reddening assuming $E(B-V) = 0.055$. We used a carefully interpolated grid of ATLAS models (e.g., Kurucz 2005) to derive the angular diameter and effective temperature of δ Vel B. We find a photospheric limb darkened angular diameter of $\theta_{\mathrm{LD}}(\mathrm{B}) = 0.530 \pm 0.011$ mas and an effective temperature of $T_{\mathrm{eff}}(\mathrm{B}) = 6600 \pm 100$ K. Based on our distance estimate, we can derive the physical radius to be $R(\mathrm{B}) = 1.43 \pm 0.03\, R_\odot$ and thus a luminosity of $L(\mathrm{B}) = 3.5 \pm 0.2\, L_\odot$. Assuming the star is on the main-sequence we can infer, based on the mass-luminosity relation by Torres, Andersen & Giménez (2010), that δ Vel B has a spectral type F7.5V and a mass of

$$M_{\mathrm{photometric}}(\mathrm{B}) = 1.35 \pm 0.1\, M_\odot. \quad (3)$$

These parameters estimated using an independent method are comparable to the values we obtained in Paper I.

Table 6. Orbital parameters of the visual pair A-B.

Parameter	This work	Argyle et al. (2002)
a ($''$)	1.996 ± 0.012	1.990 ± 0.020
e	0.475 ± 0.003	0.470 ± 0.020
Period (yr)	143.2 ± 1.2	142 ± 13
MJD_0	51774 ± 430	51836.80 ± 584
i (deg)	105.1 ± 0.2	105.20 ± 2.20
Ω (deg)	286.6 ± 0.36	287.00 ± 1.30
ω (deg)	187.4 ± 0.6	188.00 ± 14.00
$M(\mathrm{Aab + B})$ ($M_\odot$)	6.15 ± 0.23	5.88 ± 1.17

Notes. The total mass (last line) is computed using Kepler's third law, assuming the revised parallax $\pi = 39.8 \pm 0.4$ mas.

Table 7. Spectral energy density (SED) fit of δ Vel B, using our photometric measurements in the K- and N-bands (in two narrow-band filters of VISIR: PAH1 and PAH2).

Filter	Meas.	Redd.	SED $W/m^2/\mu m$	Modeled SED $W/m^2/\mu m$
V (Mag)	5.54	0.18	2.159×10^{-10}	2.143×10^{-10}
K (Mag)	4.40	0.02	6.951×10^{-12}	7.135×10^{-12}
PAH1 (flux)	0.94Jy	negl.	3.816×10^{-14}	3.816×10^{-14}
PAH2 (flux)	0.58Jy	negl.	1.369×10^{-14}	1.310×10^{-14}

Notes. The third column is the reddening correction corresponding to $E(B-V) = 0.055$. The model (last column) is for an angular diameter of 0.53 mas and effective temperature of 6600 K.

We can compare this mass estimate with the value we can compute from the mass of A ($4.69 \pm 0.03 M_\odot$ from Table 2) and A+B ($6.15 \pm 0.23\ M_\odot$ from Table 6). This leads to

$$M_{\rm dynamic}({\rm B}) = M({\rm A}+{\rm B}) - M({\rm A}) = 1.46 \pm 0.23\ M_\odot, \quad (4)$$

which is consistent with the photometric estimate (Eq. (3)).

4. Conclusion

We presented a self-consistent model of the triple stellar system δ Vel. Our model reproduces photometric, spectroscopic, and interferometric data of the eclipsing pair Aa-Ab. We determined the orbital (Table 2) and fundamental stellar parameters (Table 3) of the three components of the system. The physical properties of the eclipsing components are surprisingly similar to the A0V benchmark star Vega. Thanks to the resolution of the system using the AMBER instrument, we also independently determined the distance to the system ($\pi = 39.8 \pm 0.4$ mas, or 25.1 ± 0.25 pc), as well as the interstellar reddening value toward this nearby system, with $E(B-V) = 0.055$. The combination of two fast rotating A stars of slightly different masses and a late F-star, all coeval and with accurately measured fundamental parameters, will likely make of δ Vel a cornerstone for the study of early-type main-sequence stars.

Acknowledgements. T.P. acknowledges support from the European Union in the FP6 MC ToK project MTKD-CT-2006-042514. This work has partially been supported by VEGA project 2/0094/11. This work also received the support of PHASE, the high angular resolution partnership between ONERA, Observatoire de Paris, CNRS and University Denis Diderot Paris 7. This research has made use of the `AMBER data reduction package` of the Jean-Marie Mariotti Center[2]. This research took advantage of the SIMBAD and VIZIER databases at the CDS, Strasbourg (France), and NASA's Astrophysics Data System Bibliographic Services.

References

Aumann, H. H. 1985, PASP, 97, 885
Absil, O., Di Folco, E., Mérand, A., et al. 2006, A&A, 452, 237
Argyle, R. W., Alzner, A., & Horch, E. P. 2002, A&A, 384, 171
Aufdenberg, J. P., Mérand, A., Coudé du Foresto, V., et al. 2006, ApJ, 645, 664; Erratum 2006, ApJ, 651, 617
Castelli, F., & Kurucz, R. L. 1994, A&A, 281, 817
Chelli, A., Utrera, O. H., & Duvert, G. 2009, A&A, 502, 705
ESA 1997, The Hipparcos and Tycho Catalogues, ESA SP-1200
Gáspár, A., Su, K. Y. L., Rieke, G. H., et al. 2008, ApJ, 672, 974
Gray, R. O., Corbally, C. J., Garrison, R. F., et al. 2006, AJ, 132, 161
Grenier, S., Burnage, R., & Farragiana, R. 1999, A&AS, 135, 503
Gulliver, A. F., Hill, G., & Adelman, S. J. 1994, ApJ, 429, 81
Hempel, M., & Schmitt, J. H. M. M. 2003, A&A, 408, 971
Horch, E., Franz, O. G., & Ninkov, Z. 2000, AJ, 120, 2638
Innes, R. T. A. 1895, MNRAS, 55, 312
Kellerer, A., Petr-Gotzens, M., Kervella, P., & Coudé du Foresto, P. 2007, A&A, 469, 633
Kervella, P., Bersier, D., Mourard, D., et al. 2004, A&A, 428, 587
Kervella, P., Thévenin, F., & Petr-Gotzens M. G. 2009, A&A, 493, 107 (Paper I)
Kurucz, R. L. 2005, MmSAI Suppl., 8, 14
Lagage, P. O., Pel, J. W., Authier, M., et al. 2004, The ESO Messenger 117, 12
Lenzen, R., Hofmann, R., Bizenberger, P., & Tusche, A. 1998, SPIE, 3354, 606
Masciadri, E., Brandner, W., Bouy, H., et al. 2003, A&A, 411, 157
Mérand, A., Bordé, P., & Coudé du Foresto, V. 2005, A&A, 433, 1155
Moerchen, M. M., Telesco, C. M., & Packham, C. 2010, ApJ, 723, 1418
Monnier, J.-D., Zhao, M., Pedretti, E., et al. 2007, Science, 317, 342
Morel, M., & Magnenat, P. 1978, A&AS, 34, 477
Neuhäuser, R., Mugrauer, M., Seifahrt, A., Schmidt, T. O. B., & Vogt, N. 2008, A&A, 484, 281
Otero, S. A., Fieseler, P. D., & Lloyd, C. 2000, IBVS, 4999
Petrov, R. G., Millour, F., Chelli, A., et al. 2007, A&A, 464, 1
Pribulla, T., Mérand, A., Kervella, P., et al. 2011, A&A, 528, A21 (Paper II)
Rousset, G., Lacombe, F., Puget, F., et al. 2003, Proc. SPIE, 4839, 140
Skrutskie, R. M., Cutri, R., Stiening, M. D., et al. 2006, AJ, 131, 1163
Spreckley, S. A., & Stevens, I. R. 2008, MNRAS, 388, 1239
Su, K. Y. L., Rieke, G. H., Stapelfeldt, K. R., et al. 2008, ApJ, 679, L125
Tango, W. J., Davis, R. J., Thompson, R. J., & Hanbury Brown, R. 1979, Proc. Austr. Astro. Soc., 3, 323
Tatulli, E., Millour, F., Chelli, A., et al. 2007, A&A, 464, 29
Torres, G., Andersen, J., & Giménez, A. 2010, A&ARv, 18, 67
Van Altena, W. F., Lee, J. T., & Hoffleit, E. D. 1995, The General Catalogue of Trigonometric Stellar Parallaxes, 4th edn. (Yale University Observatory)
van Leeuwen, F. 2007, Hipparcos, the New Reduction of the Raw Data, A&SS Library (Berlin: Springer), 350
von Zeipel, H. 1924, MNRAS, 84, 665

[2] Available at http://www.jmmc.fr/amberdrs